LETTER

https://doi.org/10.1038/s41586-019-1216-1

A massive white-dwarf merger product before final collapse

Vasilii V. Gvaramadze[1,2,3]*, Götz Gräfener[4]*, Norbert Langer[4,5], Olga V. Maryeva[1,6], Alexei Y. Kniazev[1,7,8], Alexander S. Moskvitin[9] & Olga I. Spiridonova[9]

Gravitational-wave emission can lead to the coalescence of close pairs of compact objects orbiting each other[1,2]. In the case of neutron stars, such mergers may yield masses above the Tolman–Oppenheimer–Volkoff limit (2 to 2.7 solar masses)[3], leading to the formation of black holes[4]. For white dwarfs, the mass of the merger product may exceed the Chandrasekhar limit, leading either to a thermonuclear explosion as a type Ia supernova[5,6] or to a collapse forming a neutron star[7,8]. The latter case is expected to result in a hydrogen- and helium-free circumstellar nebula and a hot, luminous, rapidly rotating and highly magnetized central star with a lifetime of about 10,000 years[9,10]. Here we report observations of a hot star with a spectrum dominated by emission lines, which is located at the centre of a circular mid-infrared nebula. The widths of the emission lines imply that wind material leaves the star with an outflow velocity of 16,000 kilometres per second and that rapid stellar rotation and a strong magnetic field aid the wind acceleration. Given that hydrogen and helium are probably absent from the star and nebula, we conclude that both objects formed recently from the merger of two massive white dwarfs. Our stellar-atmosphere and wind models indicate a stellar surface temperature of about 200,000 kelvin and a luminosity of about $10^{4.6}$ solar luminosities. The properties of the star and nebula agree with models of the post-merger evolution of super-Chandrasekhar-mass white dwarfs[9], which predict a bright optical and high-energy transient upon collapse of the star[11] within the next few thousand years. Our observations indicate that super-Chandrasekhar-mass white-dwarf mergers can avoid thermonuclear explosion as type Ia supernovae, and provide evidence of the generation of magnetic fields in stellar mergers.

During our search for mid-infrared circumstellar nebulae (see Methods), we discovered a new object in the constellation Cassiopeia (Fig. 1) using data from the Wide-field Infrared Survey Explorer (WISE)[12]. At a wavelength of 22 μm the new nebula appears as a circular shell with ragged edges and an angular radius of about 75 arcsec. The higher-contrast 22-μm image of the nebula shows a diffuse halo with a radius of about 110 arcsec surrounding the shell. For a distance of about 3 kpc to the nebula (see below), the linear radii of the shell and halo are about 1.1 pc and 1.6 pc, respectively. The shell is also visible in the WISE 12-μm image, where it appears as a circular diffuse structure of the same angular size as the 22-μm shell. Surprisingly, despite the moderate extinction towards the nebula (see below), the shell has no optical counterpart in the INT Photometric Hα Survey (IPHAS) of the Northern Galactic Plane[13] (see Fig. 1). We identified the central star of the nebula with an optical star ($V \approx 15.5$ mag) located at RA = 00 h 53 min 11.21 s and dec. = +67° 30′ 2.1″ (J2000). In the following, we call this star J005311 (see Methods).

Optical follow-up spectroscopy of J005311 with the Russian 6-m telescope (see Methods) revealed an emission-line-dominated spectrum, reminiscent of oxygen-rich Wolf–Rayet (WO type) stars (Fig. 2). However, the emission lines of J005311 are stronger and broader than those of even the most extreme (in terms of strength and width of their emission lines) WO stars. Most notably, the O VI (3,811 Å, 3,834 Å) emission doublet shows an equivalent width of EW(O VI) ≈ 2,300 Å and a full-width at half-maximum of about 300 Å. We note that no nebular lines are visible in the obtained long-slit spectrum.

We analysed the optical spectrum of J005311 using the Potsdam Wolf–Rayet code for expanding stellar atmospheres (see Methods). In Fig. 2, we compare our best-fitting model with the observed spectrum. The line spectrum is reproduced well, except for two missing emission lines near 4,340 Å and 6,068 Å, which are probably formed by high-lying transitions of highly ionized oxygen (O VIII) or neon (Ne VIII) ions. The lines may either originate from a hot plasma that coexists with the cooler simulated wind material in our models, or indicate a high neon abundance (see Methods). Our model fit yields a stellar temperature of $211,000^{+40,000}_{-23,000}$ K (see footnote of Table 1 for the definition of the uncertainties) at the base of the wind and a chemical composition

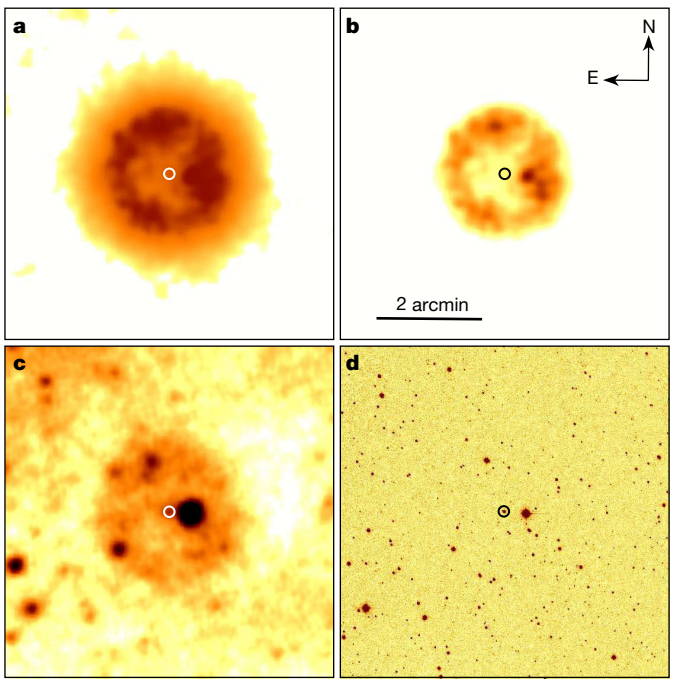

Fig. 1 | New mid-infrared nebula in Cassiopeia. a, **b**, WISE 22-μm image of the nebula at two intensity scales, highlighting details of its structure. The position of the central star J005311 is indicated by a circle. **c**, **d**, WISE 12-μm (**c**) and IPHAS Hα (**d**) images of the nebula and its central star. At the distance of J005311 (about 3 kpc), 1 arcmin corresponds to about 0.9 pc. All images have the same angular scale and orientation.

[1]Sternberg Astronomical Institute, Lomonosov Moscow State University, Moscow, Russia. [2]Space Research Institute, Russian Academy of Sciences, Moscow, Russia. [3]Isaac Newton Institute of Chile, Moscow Branch, Moscow, Russia. [4]Argelander-Institut für Astronomie, Universität Bonn, Bonn, Germany. [5]Max-Planck-Institut für Radioastronomie, Bonn, Germany. [6]Astronomický ústav, Akademie věd České Republiky, Ondejov, Czech Republic. [7]South African Astronomical Observatory, Cape Town, South Africa. [8]Southern African Large Telescope Foundation, Cape Town, South Africa. [9]Special Astrophysical Observatory of the Russian Academy of Sciences, Nizhnii Arkhyz, Russia. *e-mail: vgvaram@mx.iki.rssi.ru; goetz@astro.uni-bonn.de

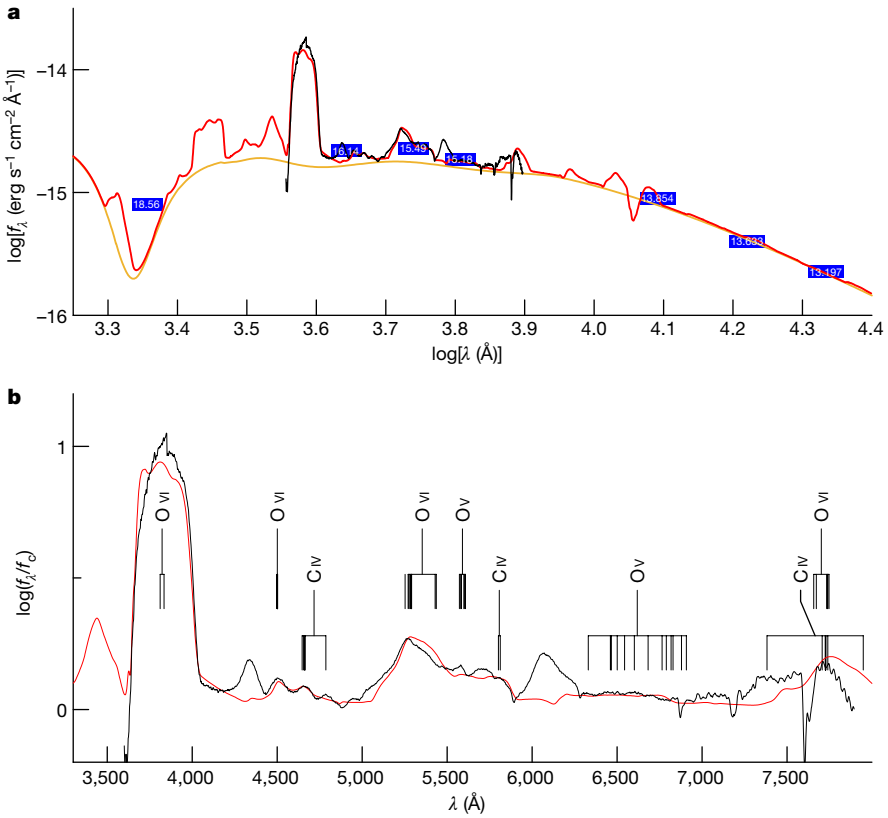

Fig. 2 | Spectral modelling of J005311. a, Observed flux distribution of J005311 in absolute units, including the calibrated spectrum (black line) and photometric measurements (blue rectangles), compared to our best-fitting model spectrum (red line) and model continuum (orange line). The modelled flux has been reddened and scaled to the distance according to the parameters given in Table 1. f_c, model continuum flux. **b**, Observed optical spectrum of J005311 (black line), compared with our best-fitting model (red line), both divided by the theoretical continuum flux. Spectral lines that contribute substantially to the model spectrum are highlighted.

dominated by oxygen and carbon with mass fractions of 0.8 ± 0.1 and 0.2 ± 0.1, respectively, in line with white-dwarf core abundances recently obtained from asteroseismology[14]. Remarkably, the absence of the He II 4,686 Å emission line implies an essentially helium-free composition, with a conservative upper limit of 0.1 on the helium surface mass fraction. From the width of the O VI (3,811 Å, 3,834 Å) emission we derive a terminal wind velocity of $v_\infty = 16{,}000 \pm 1{,}000$ km s^{-1}. The strength of the emission lines is best reproduced with a mass-loss rate of $\dot{M} = (3.5 \pm 0.6) \times 10^{-6} M_\odot$ yr^{-1} (where $M_\odot$ is the solar mass) with a wind clumping factor of 10 (Methods).

Using the distance to J005311 of $3.07^{+0.34}_{-0.28}$ kpc derived from the second Gaia data release[15], our model reproduces the observed flux distribution from the ultraviolet to the infrared with a luminosity L_* described by $\log(L_*/L_\odot) = 4.60 \pm 0.14$ (where $L_\odot$ is the solar luminosity) and with an interstellar extinction of $E(B-V) = 0.835 \pm 0.035$ mag (see Fig. 2 and Methods). This luminosity is four times lower than those of even the faintest massive WO-type Wolf–Rayet stars[16] ($\log(L_*/L_\odot) > 5.2$) and at least about four times higher than those of the known low-mass (WO-type) central stars of planetary nebulae[17] ($\log(L_*/L_\odot) < 4.0$).

Very few hot stars free of hydrogen and helium are known in the Milky Way. Besides the rare DQ white dwarfs[18], there are two hot white dwarfs with unusually high masses ($0.7 M_\odot$–$1.0 M_\odot$), which have been suggested to have formed through the merger of two carbon–oxygen white dwarfs[19]. Recent models for the evolution of super-Chandrasekhar-mass carbon–oxygen white-dwarf merger remnants[9] match the properties of J005311 remarkably well. First, the fiducial model of such remnants comes close to the Hertzsprung–Russell diagram position of J005311 (Fig. 3). Second, these models predict an episode of extreme mass loss during and shortly after a merger event in an expanded cool phase, which forms a hydrogen- and helium-free circumstellar nebula with a slow expansion velocity of about 100 km s^{-1}. The expected hydrogen- and helium-free composition of the nebula and the high temperature of its central star (leading to triple ionization of oxygen) suggest that no optical nebular lines form, and that the observed mid-infrared emission from the nebula around J005311 is dominated by the [O IV] 25.89 μm and [Ne V] 14.32 μm and 24.32 μm lines[20].

Table 1 | Stellar parameters and surface abundances of J005311

Parameter	Value
$\log(L_*/L_\odot)$	4.60 ± 0.14
T_* (K)	$211{,}000^{+40{,}000}_{-23{,}000}$
R_* ($R_\odot$)	0.15 ± 0.04
$\dot{M}$ ($M_\odot$ yr^{-1})	$(3.5 \pm 0.6) \times 10^{-6}$
D	10
v_∞ (km s^{-1})	$16{,}000 \pm 1{,}000$
β	1.0
d (kpc)	$3.07^{+0.34}_{-0.28}$
$E(B-V)$ (mag)	0.835 ± 0.035
R_V	3.1
He mass fraction	<0.1
C mass fraction	0.2 ± 0.1
O mass fraction	0.8 ± 0.1
Ne mass fraction	0.01
Fe group mass fraction	1.6×10^{-3}

The given uncertainties are an indicator of the obtained fit quality as a function of stellar parameters, on the basis of the criteria described in Methods. Owing to the nature of this analysis they do not represent statistical error distributions. Parameters without error estimates were adopted in the model. D, wind clumping factor; β, acceleration parameter; d, distance to J005311; R_V, total-to-selective absorption ratio.

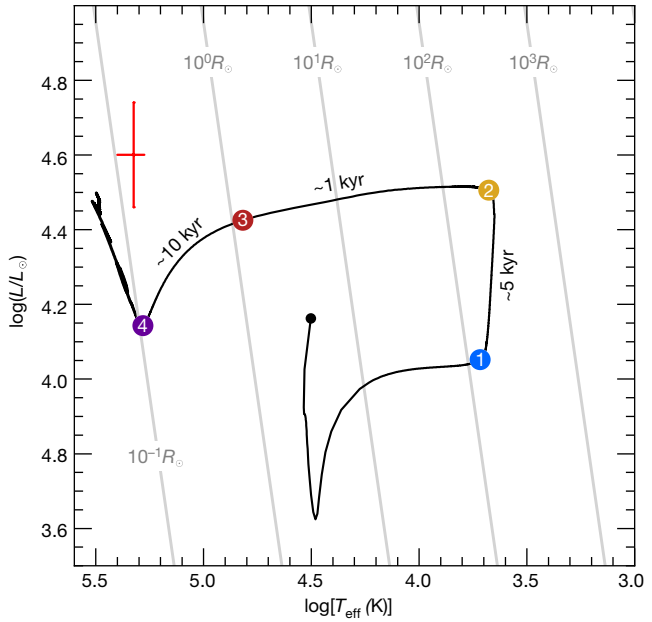

Fig. 3 | Position of J005311 in the Hertzsprung–Russell diagram. The red cross marks the position of J005311, with error bars (see Table 1). This position is compared with the evolutionary track of the fiducial carbon–oxygen white-dwarf post-merger model[9], which starts at the black dot and passes through the points labelled 1, 2, 3 and 4, which correspond to about 100, 5,000, 6,000 and 16,000 yr, respectively, after the merger. Figure adapted from ref. [9] with permission from Oxford University Press.

This naturally explains why this nebula appears neither in the IPHAS image nor in our long-slit spectrum. The possibility of a high neon surface abundance could even imply that a high-mass neon–oxygen white dwarf participated in the merger event.

The merging white-dwarf scenario also addresses the extremely large width of the emission lines of J005311. A velocity of 16,000 km s^{-1} exceeds the stellar escape speed by about eight times and is typical for supernovae, but so far unheard of for radiation-driven winds. In fact, pure radiation driving is excluded because the wind's kinetic energy flux exceeds the total radiative luminosity of the star by a factor of two (Methods). However, this extremely high velocity can be explained in the framework of rotating magnetic wind models. It has been found[21] that a rigidly co-rotating magnetic field can increase the speed and mass outflow rate of radiation-driven winds by more than a factor of three, at the cost of the star's rotational energy. We find that a co-rotation speed of 16,000 km s^{-1} at the Alfvén point in J005311, where the inertia force starts to dominate over the magnetic forces[22], requires an Alfvén radius of about 10 stellar radii (about $1.5R_\odot$; $R_\odot$, solar radius), which is achieved with a magnetic field strength of about 10^8 G. Because the whole post-merger evolution is expected[9] to last about 20,000 yr, it is plausible that the corresponding magnetic torques have not yet spun down J005311.

The generation of a strong magnetic field is indeed expected in stellar mergers[23]. Three-dimensional magneto-hydrodynamical models of white-dwarf mergers find[10] a magnetization of the merger product of 2×10^8 G. This compares to the peak of the magnetic-field distribution of magnetic white dwarfs[24], which is several tens of megagauss. The observations that the mean mass of magnetic white dwarfs is considerably higher than that of non-magnetic ones and that nearly none of the known magnetic white dwarfs have a companion star provide strong evidence for the generation of magnetic fields by the merging of white dwarfs[24].

With a wind speed of about 100 km s^{-1} during the cool phase[8], the angular radius of 1.6 pc of the nebula implies an expansion age of about 16,000 yr. This, together with the high stellar temperature, indicates that J005311 is close to the endpoint of its post-merger evolution. Because J005311 is more luminous than the $1.49M_\odot$ model[9], it appears likely that its mass also exceeds the Chandrasekhar limit, with the exciting perspective that it will produce a low-mass neutron star in the near future, accompanied by a high-energy transient and a fast-evolving supernova[11].

The merging of two stars in a binary system is not a rare event. About 10% of the massive main-sequence stars[25], and a similar fraction of the known white dwarfs[26], are thought to be merger products. The very unusual wind of J005311 strongly supports the idea that stellar mergers can indeed produce highly magnetized stars, which would explain the magnetic stars of the upper main sequence[27] and the formation of magnetic white dwarfs[24]. Our results may also help to resolve the ongoing debate on whether a super-Chandrasekhar-mass merger of two carbon–oxygen white dwarfs leads to a type Ia supernova, for which J005311 appears to provide a counter-example, indicating that the merger produced enough heat to prevent immediate collapse and to ignite carbon non-explosively. The sequence of thermonuclear burning stages was thus only interrupted during the white-dwarf stage of both components and is now expected to continue and to end in a core collapse within the next few thousand years[9]. This will probably produce a neutrino flash and a γ-ray burst[28], followed by a very fast and subluminous type Ic supernova[11].

Online content

Any methods, additional references, Nature Research reporting summaries, source data, statements of data availability and associated accession codes are available at https://doi.org/10.1038/s41586-019-1216-1.

Received: 15 June 2018; Accepted: 28 March 2019;
Published online 20 May 2019.

1. Hulse, R. A. & Taylor, J. H. Discovery of a pulsar in a binary system. *Astrophys. J.* **195**, L51–L53 (1975).
2. Abbott, B. P. et al. Observation of gravitational waves from a binary black hole merger. *Phys. Rev. Lett.* **116**, 061102 (2016).
3. Özel, F. & Freire, P. Masses, radii, and the equation of state of neutron stars. *Annu. Rev. Astron. Astrophys.* **54**, 401–440 (2016).
4. Abbott, B. P. et al. Gravitational waves and gamma-rays from a binary neutron star merger: GW170817 and GRB 170817A. *Astrophys. J.* **848**, L13 (2017).
5. Iben, I. & Tutukov, A. V. Supernovae of type I as end products of the evolution of binaries with components of moderate initial mass ($M \leq 9M_\odot$). *Astron. Astrophys. Suppl. Ser.* **54**, 335–372 (1984).
6. Pakmor, R. et al. Violent mergers of nearly equal-mass white dwarf as progenitors of subluminous Type Ia supernovae. *Astron. Astrophys.* **528**, A117 (2011).
7. Saio, H. & Nomoto, K. Off-center carbon ignition in rapidly rotating, accreting carbon-oxygen white dwarfs. *Astrophys. J.* **615**, 444–449 (2004).
8. Shen, K. J., Bildsten, L., Kasen, D. & Quataert, E. The long-term evolution of double white dwarf mergers. *Astrophys. J.* **748**, 35 (2012).
9. Schwab, J., Quataert, E. & Kasen, D. The evolution and fate of super-Chandrasekhar mass white dwarf merger remnants. *Mon. Not. R. Astron. Soc.* **463**, 3461–3475 (2016).
10. Ji, S. et al. The post-merger magnetized evolution of white dwarf binaries: the double-degenerate channel of sub-Chandrasekhar Type Ia supernovae and the formation of magnetized white dwarfs. *Astrophys. J.* **773**, 136 (2013).
11. Dessart, L. et al. Multidimensional simulations of the accretion-induced collapse of white dwarfs to neutron stars. *Astrophys. J.* **644**, 1063–1084 (2006).
12. Wright, E. L. et al. The Wide-field Infrared Survey Explorer (WISE): mission description and initial on-orbit performance. *Astron. J.* **140**, 1868–1881 (2010).
13. Drew, J. E. et al. The INT Photometric Hα Survey of the Northern Galactic Plane (IPHAS). *Mon. Not. R. Astron. Soc.* **362**, 753–776 (2005).
14. Giammichele, N. et al. A large oxygen-dominated core from the seismic cartography of a pulsating white dwarf. *Nature* **554**, 73–76 (2018).
15. Bailer-Jones, C. A. L., Rybizki, J., Fouesneau, M., Mantelet, G. & Andrae, R. Estimating distances from parallaxes IV: distances to 1.33 billion stars in Gaia Data Release 2. *Astron. J.* **156**, 58 (2018).
16. Tramper, F. et al. Massive stars on the verge of exploding: the properties of oxygen sequence Wolf–Rayet stars. *Astron. Astrophys.* **581**, A110 (2015).
17. Gesicki, K. et al. Planetary nebulae with emission-line central stars. *Astron. Astrophys.* **451**, 925–935 (2006).
18. Dufour, P., Liebert, J., Fontaine, G. & Behara, N. White dwarf stars with carbon atmospheres. *Nature* **450**, 522–524 (2007).
19. Werner, K. & Rauch, T. Analysis of HST/COS spectra of the bare C–O stellar core H1504+65 and a high-velocity twin in the Galactic halo. *Astron. Astrophys.* **584**, A19 (2015).
20. Flagey, N., Noriega-Crespo, A., Billot, N. & Carey, S. J. Spitzer/infrared spectrograph investigation of MIPSGAL 24 μm compact bubbles. *Astrophys. J.* **741**, 4 (2011).
21. Poe, C. H., Friend, D. B. & Cassinelli, J. P. A rotating, magnetic, radiation-driven wind model for Wolf–Rayet stars. *Astrophys. J.* **337**, 888–902 (1989).

22. Petit, V. et al. A magnetic confinement versus rotation classification of massive-star magnetospheres. *Mon. Not. R. Astron. Soc.* **429**, 398–422 (2013).
23. Beloborodov, A. M. Magnetically powered outbursts from white dwarf mergers. *Mon. Not. R. Astron. Soc.* **438**, 169–176 (2014).
24. Wickramasinghe, D. T. & Ferrario, L. Magnetism in isolated and binary white dwarfs. *Publ. Astron. Soc. Pacif.* **112**, 873–924 (2000).
25. de Mink, S. E., Sana, H., Langer, N., Izzard, R. G. & Schneider, F. R. N. The incidence of stellar mergers and mass gainers among massive stars. *Astrophys. J.* **782**, 7 (2014).
26. Maoz, D., Hallakoun, N. & Badenes, C. The separation distribution and merger rate of double white dwarfs: improved constraints. *Mon. Not. R. Astron. Soc.* **476**, 2584–2590 (2018).
27. Fossati, L. et al. Evidence of magnetic field decay in massive main-sequence stars. *Astron. Astrophys.* **592**, A84 (2016).
28. Dar, A., Kozlovsky, B. Z., Nussinov, S. & Ramaty, R. Gamma-ray bursts and cosmic rays from accretion-induced collapse. *Astrophys. J.* **388**, 164–170 (1992).

Acknowledgements We thank T. Rauch and K. Werner for discussions and for providing atomic data through the Tübingen Model Atom Database in the framework of the German Virtual Observatory. V.V.G. acknowledges support from the Russian Science Foundation under grant 14-12-01096 and from the Russian Foundation for Basic Research (RFBR) under grant 19-02-00779. G.G. acknowledges financial support from Deutsche Forschunsgemeinschaft (DFG) under grant GR 1717/5-1. O.V.M. acknowledges support from RFBR under grant 16-02-00148 and from the Czech Science Foundation under grant GA ČR 18-05665S. A.Y.K. acknowledges support from RFBR under grant 16-02-00148 and from the National Research Foundation (NRF) of South Africa. The TMAD tool (http://astro.uni-tuebingen.de/~TMAD) used in this study was constructed as part of the activities of the German Astrophysical Virtual Observatory. This research made use of the SIMBAD database, operated at CDS, Strasbourg, France.

Author contributions V.V.G., G.G. and N.L. jointly analysed and interpreted observational data and wrote the manuscript. O.V.M. obtained and reduced the spectroscopic material. A.Y.K. provided ideas for the interpretation of the nebula. A.S.M. and O.I.S. obtained optical photometry data. All authors discussed the results and commented on the manuscript.

Competing interests The authors declare no competing interests.

Additional information
Extended data is available for this paper at https://doi.org/10.1038/s41586-019-1216-1.
Reprints and permissions information is available at http://www.nature.com/reprints.
Correspondence and requests for materials should be addressed to V.V.G. or G.G.
Publisher's note: Springer Nature remains neutral with regard to jurisdictional claims in published maps and institutional affiliations.

METHODS

Observations. We discovered a new nebula in Cassiopeia in a search for evolved massive stars through the detection of their mid-infrared circumstellar nebulae[29,30]. This nebula coincides with the IRAS source IRAS 00500+6713, which in the SIMBAD database[31] (http://simbad.u-strasbg.fr/simbad/) is erroneously associated with the brightest star in the field, TYC 4296-1313-1. At the very centre of the nebula we identified a faint point source as the central star (see Fig. 1). This star is listed as IPHAS J005311.21+673002.1 in the IPHAS DR2 Source Catalogue[32]. The coordinates of the star are given in the main text, and we use the short name J005311 throughout this paper.

J005311 was observed with the 6-m telescope of the Special Astrophysical Observatory of the Russian Academy of Science (SAO RAS) using the Spectral Camera with Optical Reducer for Photometric and Interferometric Observations (SCORPIO)[33] on 2017 July 20. The spectrum was obtained in the long-slit mode with a slit width of 1 arcsec, using the grism VRHG550G. This spectral setup covered a wavelength range of about 3,600–7,800 Å with a spectral resolution of 12 Å (estimated using the spectra of a He–Ar–Ne lamp). Three images with exposures of 10 min were taken with a seeing of about 1.5 arcsec. For flux calibration the spectrophotometric standard star[34] BD+33° 2642 was observed. The spectrum was reduced using the ScoRe package, which incorporates all the standard stages of SCORPIO long-slit data reduction[35].

To obtain contemporary photometry data of J005311 and to examine them for possible variability, we observed this star in the B, V and R_c filters using the charge-coupled device photometer of the 1-m Zeiss-1000 telescope of SAO RAS. Nine measurements were carried out in the period from 2017 August 18 to 2018 April 30. We found that the brightness of J005311 varies by $\leq$0.05 mag around mean values of $B = 16.14 \pm 0.02$ mag, $V = 15.49 \pm 0.01$ mag and $R_c = 15.18 \pm 0.01$ mag. We used these values to model the spectral energy distribution (SED) of J005311 (see next section).

Spectral analysis. J005311 displays an extremely early WO-type emission-line spectrum, which implies a very high temperature, and a carbon- and oxygen-dominated surface composition. On the basis of the equivalent widths of the primary classification lines O VI (3,811 Å, 3,834 Å) (with EW(O VI) $\approx$ 2,300 Å) and O V 5,590 Å (with EW(O V) $\leq$ 120 Å), we derive the ratio log[EW(O VI)/EW(O V)] $\geq$ 1.3, which puts[36] J005311 in the earliest WO sub-class, WO1. In addition, J005311 shows two emission lines near 4,340 Å and 6,068 Å. In previous spectroscopic works[37,38] on WO and PG1159 stars, these lines appeared much weaker and were identified as hydrogen- and helium-like ions of oxygen (O VII, O VIII) or neon (Ne VIII). However, although the two lines were successfully modelled using Ne VIII in static models of PG1159 stars, they have not been reproduced by any previous models[16,39] for WO stars with strong stellar winds.

We performed a quantitative spectroscopic analysis of J005311 using non-LTE (local thermodynamic equilibrium) model atmospheres for Wolf–Rayet stars[40–42]. Our models include model atoms for He II–III, C IV–VII, O IV–VIII, Ne IV–IX and the Fe group (ionization stages V–IX of Sc, Ti, V, Cr, Mn, Fe, Co and Ni, combined in a generic model atom with fixed relative abundances corresponding to the solar metal distribution, and Fe up to Fe XVII; see refs. [41,43] for a detailed description of the included atomic data).

Compared with previous WC models we extended the present models to include the continuum opacities of the high-ionization stages C V and O VII, to prevent the models from becoming translucent in the X-ray range, and included the ions Ne IV–IX. For Ne IV–VII our models are based on theoretical data from the Opacity Project database[44], with corrected fine-structure level energies taken from the database of the National Institute of Standards and Technology[45]. Our non-LTE model atoms comprise the lowest 7, 12, 16 and 13 energy levels of Ne IV–VII, plus one auxiliary level in which all higher-lying levels are combined, for each ion. In the final computation of the emergent spectrum in the observer's frame, the non-LTE levels are split into their fine-structure components. For Ne VIII we followed a different approach because the relevant optical line transitions are not included in the Opacity Project data. We therefore used fine-structure data from the Tübingen Model Atom Database (http://astro.uni-tuebingen.de/~TMAD/). From the 120 available energy levels we treated the lowest 24 (main quantum numbers $n = 1$–5) explicitly, and combined the higher-lying levels ($n = 6$–11) into one level for each n. Again, all fine-structure levels were treated separately in the observer's-frame computation.

Our models are the first models for WO stars that include the opacities of the Fe M-shell ions (Fe IX–XVI), which are responsible for the Fe-opacity peak that arises near temperatures[46] of about 150,000 K. In previous models for WC stars, the opacities of the Fe group were found to dominate the flux-mean opacity throughout the atmosphere/wind, with the Fe peak opacities being crucial for the formation of the observable O VI (3,811 Å, 3,834 Å) feature at high temperatures[43]. We further assumed a clumped wind structure and a β-type velocity law with a fixed acceleration parameter $\beta = 1$, and included line broadening with a fixed Doppler broadening velocity of $v_D = 250$ km s^{-1}.

In our analysis we determined the stellar temperature T_*, the surface abundances and the wind parameters from the observed line spectrum of J005311 using a combination of model grids and manual model fits. Our initial analysis was based on a grid of models containing He, C, O and the elements of the Fe group, covering a range of $T_* \approx$ 160–560 kK and $\log[\dot{M}/M_\odot(\mathrm{yr}^{-1})]$ between -5.2 and -6.1. After matching the line spectrum, we adjusted the stellar luminosity L_* to match the observed SED, taking advantage of scaling relations[41] between $\dot{M}$ and L_*. After this initial analysis we determined the final parameters given in Table 1 using models containing C, O, Ne and the elements of the Fe group, covering a temperature range of $T_* = 170$–270 kK, and mass-loss rates $\log[\dot{M}/M_\odot(\mathrm{yr}^{-1})]$ between about -5.4 and -5.7.

The SED was fitted using the extinction law[47] with a total-to-selective absorption ratio of $R_V = 3.1$. The observed SED was constructed from the flux-calibrated spectrum and photometric data. Besides our own optical photometry, we used the Galaxy Evolution Explorer (GALEX) near-ultraviolet magnitude of 18.56 ± 0.05 from the Mikulski Archive for Space Telescopes (MAST; https://archive.stsci.edu/) and the (J, H, K_s) magnitudes of (13.85 ± 0.03, 13.63 ± 0.04, 13.20 ± 0.04) from the Two-Micron All Sky Survey (2MASS) All-Sky Catalog of Point Sources[48]. Because the ultraviolet-to-optical flux distribution is substantially affected by interstellar extinction, the derived luminosity of J005311 relies mainly on the continuum fit in the near-infrared range (see Fig. 2). We had to adjust the slope of the spectrum to match the photometric data. This was done by applying a linear correction to the observed logarithmic flux, ranging from 0.0 dex at $\log[\lambda\,(\text{Å})] = 4.0$ to 0.11 dex at $\log[\lambda\,(\text{Å})] = 3.5$.

The wind velocity of $v_\infty = 16{,}000 \pm 1{,}000$ km s^{-1} was predominantly determined from the width of the strong O VI 3,811–3,834 Å line. This value was further backed up by the width of the O V 5,590 Å line. In our models oxygen shows a pronounced onion-shell structure where O V is the leading ion in the outer layers, followed by O VI and O VII further inwards. As a consequence, O V 5,590 Å shows a very broad, almost rectangular, flat-top line profile, as is expected for optically thin emission from a hollow shell. While the blue part of this line profile is blended with O VI 5,300 Å, its red edge is clearly visible near 5,900 Å, supporting the high value of v_∞ derived in this work.

To investigate the origin of the two emission lines near 4,340 Å and 6,068 Å we used grid models with neon surface mass fractions between 0.1% and 50%. For mass fractions of 0.1% and 1% our models show only marginal neon features. For values of about 10% and higher our models produce clearly visible neon features, namely, Ne VII 3,644 Å, Ne VII 3,860–3,919 Å, Ne VIII 4,340 Å, Ne VIII 6,068 Å and Ne VIII (6,894 Å, 6,993 Å). The two Ne VII lines are overlapping with the much stronger O VI 3,811–3,834 Å line, so they cannot be used for spectroscopic diagnostics.

To match the strength of the observed emission lines near 4,340 Å and 6,068 Å it is necessary to increase the neon abundance to about 50%. However, as demonstrated in Extended Data Fig. 1, with such high neon abundances our models produce carbon and oxygen features that are too weak and neon line profiles that do not match the observations. Moreover, we predict a strong Ne VIII feature at 6,894–6,993 Å that is not observed. Therefore, on the basis of our analysis it seems unlikely that the two emission lines originate from neon, although we cannot exclude that the—presumably aspherical—wind geometry of J005311 could somehow account for the discrepancies. On the other hand, O VIII is not excited in sufficient amounts in our models to explain the observed features through direct wind emission.

As a consequence, there are two possibilities: if the surface composition of J005311 is dominated by neon with an abundance of the order of 50%, at least the strength of the features near 4,340 Å and 6,068 Å could be explained by wind emission; if the neon abundance is lower, as implied by our analysis, the surface composition would be dominated by oxygen. In that case, the observed features could be explained by recombination from O IX to O VIII in a fully ionized plasma. Such a hot plasma could be produced by wind shocks and coexist with the cooler wind material that we are modelling in our spectral synthesis code. Notably, the impact of the Ne abundance on the observed flux distribution, and thus on the derived luminosity of J005311, is negligible (see Extended Data Fig. 1). For our spectral analysis of J005311 we adopted a Ne surface mass fraction of 1% and neglected the observed lines near 4,340 Å and 6,068 Å.

For the helium mass fraction we determined an upper limit of $Y < 0.1$ on the basis of the absence of He II 4,686 Å in the observed spectrum of J005311. Extended Data Fig. 2a shows that this line forms a broad emission feature with a sharp peak at its rest wavelength if helium is included with mass fractions of $Y = 0.1$ and 0.2, compared with our best-fitting model without helium. Extended Data Fig. 2b shows how changes in the carbon abundance affect the spectrum in the same wavelength range. The small C IV emission feature near 4,660 Å is the only carbon emission line that we could clearly identify in the observed spectrum. Using its strength relative to the neighbouring O VI line at 4,500 Å, we determined a carbon mass fraction of $X(\mathrm{C}) = 0.2 \pm 0.1$.

The mass-loss rate $\dot{M}$ was constrained by the strength of the O v 5,590 Å line, which reacts very sensitively to changes in the wind density. However, we note that there is a degeneracy between $\dot{M}$ and the wind clumping factor D, with $\dot{M}\sqrt{D}$ = constant, where D can only be determined very roughly from the strength of the electron-scattering wings of strong emission lines[49]. For J005311 the red wing of the O VI 3,811–3,834 Å emission implies $D \geq 10$. In our analysis, we adopt $D = 10$, which is a typical value found in studies of emission-line stars[16,50]. However, the uncertainties are large and may affect the derived mass-loss rate by up to a factor of two.

Finally, the stellar temperature T_* was constrained by the strength and profile shape of the O VI 3,811–3,834 Å, O VI 4,500 Å and C IV 4,660 Å lines. In Extended Data Fig. 3, we show how the profile shape of these lines and the strength of O V 5,590 Å are affected by changes in T_*. The models shown are our best-fitting model compared with grid models that lie just outside the temperature range given in Table 1. Owing to different formation depths at different temperatures the profile of O VI 3,811–3,834 Å changes from triangular for the coolest model, where the line is formed at low velocities near the surface of the star, to a flat-top profile for the hottest model, where the line is formed at large velocities in the outer wind. In a similar manner, the line profiles of O VI 4,500 Å and C IV 4,660 Å change from narrow to broad. In addition, the strength of O V 5,590 Å increases strongly for the cool model.

Wind velocity of J005311. The extremely high wind velocity of J005311 ($v_\infty = 16{,}000$ km s^{-1}) is very unusual for Wolf–Rayet-type winds. For WC/WO stars, typical ratios of $v_\infty/v_{\rm esc} \approx 1.3$ (where $v_{\rm esc}$ is the escape velocity) were found[51]. Such a fixed ratio is also supported by the theory of optically thick radiatively driven winds[52]. For J005311 this would imply an escape velocity of 12,000 km s^{-1} or slightly lower if we consider that some WO stars show[51] slightly higher ratios of $v_\infty/v_{\rm esc}$.

A mass of the order of $M_* = 1.5M_\odot$ for J005311 (see main text) would imply a stellar radius of $R_* = 2GM/v_{\rm esc}^2 \geq 0.004R_\odot$ (G, gravitational constant), which is a factor of 40 lower than the value derived in our analysis (about $0.15R_\odot$). This discrepancy indicates that a different wind-driving mechanism from that of ordinary Wolf–Rayet stars is in action, that is, the wind of J005311 cannot be driven by radiation pressure alone.

This conclusion is further supported by the high mechanical wind luminosity of J005311 of $L_{\rm wind} = \dot{M}(v_\infty^2/2 + M_*G/R_*) = 8 \times 10^4 L_\odot$. This value is two times higher than the radiative luminosity L_* that we derived in our analysis, that is, the wind energy exceeds the maximum limit of $L_{\rm wind} = L_*$ that can be achieved by radiative driving. Even considering the uncertainties in $\dot{M}$ due to wind clumping, this makes it very unlikely that the wind of J005311 is radiatively driven. In fact, the radiative acceleration computed within our wind models provides only 5% of the work that is necessary to drive the wind—a value that is remarkably small compared to previous studies[41,43] of the wind dynamics of WC stars, in which agreement within 50% was achieved. Therefore, a magnetically supported, rotating wind appears to be required to explain the high wind velocity observed for J005311.

Data availability

All data and codes that support the findings of this study are available upon request from the corresponding co-authors.

29. Gvaramadze, V. V., Kniazev, A. Y. & Fabrika, S. Revealing evolved massive stars with Spitzer. *Mon. Not. R. Astron. Soc.* **405**, 1047–1060 (2010).
30. Gvaramadze, V. V. et al. Discovery of two new Galactic candidate luminous blue variables with Wide-field Infrared Survey Explorer. *Mon. Not. R. Astron. Soc.* **421**, 3325–3337 (2012).
31. Wenger, M. et al. The SIMBAD astronomical database. The CDS reference database for astronomical objects. *Astron. Astrophys.* **143**, 9–22 (2000).
32. Barentsen, G. et al. The second data release of the INT Photometric Hα Survey of the Northern Galactic Plane (IPHAS DR2). *Mon. Not. R. Astron. Soc.* **444**, 3230–3257 (2014).
33. Afanasiev, V. L. & Moiseev, A. V. The SCORPIO universal focal reducer of the 6-m telescope. *Astron. Lett.* **31**, 194–204 (2005).
34. Oke, J. B. Faint spectrophotometric standard stars. *Astron. J.* **99**, 1621–1631 (1990).
35. Maryeva, O. & Abolmasov, P. *ScoRe – Package for Long-Slit Spectroscopic Data Reduction*; http://www.sao.ru/hq/ssl/maryeva/score.html.
36. Crowther, P. A., De Marco, O. & Barlow, M. J. Quantitative classification of WC and WO stars. *Mon. Not. R. Astron. Soc.* **296**, 367–378 (1998).
37. Werner, K., Rauch, T. & Kruk, J. W. Identification of Ne VIII lines in H-deficient (pre-) white dwarfs: a new tool to constrain the temperature of the hottest stars. *Astron. Astrophys.* **474**, 591–597 (2007).
38. Torres, A. V. & Massey, P. An atlas of optical spectrophotometry of Wolf-Rayet carbon and oxygen stars. *Astrophys. J. Suppl. Ser.* **65**, 459–483 (1987).
39. Tramper, F. et al. On the nature of WO stars: a quantitative analysis of the WO3 star DR1 in IC 1613. *Astron. Astrophys.* **559**, A72 (2013).
40. Koesterke, L., Hamann, W.-R. & Gräfener, G. Expanding atmospheres in non-LTE. Radiation transfer using short characteristics. *Astron. Astrophys.* **384**, 562–567 (2002).
41. Gräfener, G., Koesterke, L. & Hamann, W.-R. Line-blanketed model atmospheres for WR stars. *Astron. Astrophys.* **387**, 244–257 (2002).
42. Hamann, W.-R. & Gräfener, G. A temperature correction method for expanding atmospheres. *Astron. Astrophys.* **410**, 993–1000 (2003).
43. Gräfener, G. & Hamann, W.-R. Hydrodynamic model atmospheres for WR stars. Self-consistent modeling of a WC star wind. *Astron. Astrophys.* **432**, 633–645 (2005).
44. Cunto, W., Mendoza, C., Ochsenbein, F. & Zeippen, C. J. Topbase at the CDS. *Astrophys. J.* **275**, L5–L8 (1993).
45. Kramida, A. et al. *NIST Atomic Spectra Database (v. 5.6.1)* (National Institute of Standards and Technology, Gaithersburg, 2013); http://physics.nist.gov/asd.
46. Iglesias, C. A. & Rogers, F. J. Updated Opal opacities. *Astrophys. J.* **464**, 943–953 (1996).
47. Cardelli, J. A., Clayton, G. C. & Mathis, J. S. The determination of ultraviolet extinction from the optical and near-infrared. *Astrophys. J.* **329**, L33–L37 (1988).
48. Cutri, R. M. et al. *2MASS All-Sky Catalog of Point Sources VizieR Online Data Catalog 2246* (2003); http://vizier.u-strasbg.fr/viz-bin/VizieR?-source=II/246.
49. Hamann, W.-R. & Koesterke, L. Spectrum formation in clumped stellar winds: consequences for the analyses of Wolf–Rayet spectra. *Astron. Astrophys.* **335**, 1003–1008 (1998).
50. Bestenlehner, J. M. et al. The VLT-FLAMES Tarantula Survey. XVII. Physical and wind properties of massive stars at the top of the main sequence. *Astron. Astrophys.* **570**, A38 (2014).
51. Gräfener, G. & Vink, J. S. Stellar mass-loss near the Eddington limit. Tracing the sub-photospheric layers of classical Wolf–Rayet stars. *Astron. Astrophys.* **560**, A6 (2013).
52. Gräfener, G., Owocki, S. P., Grassitelli, L. & Langer, N. On the optically thick winds of Wolf–Rayet stars. *Astron. Astrophys.* **608**, A34 (2017).

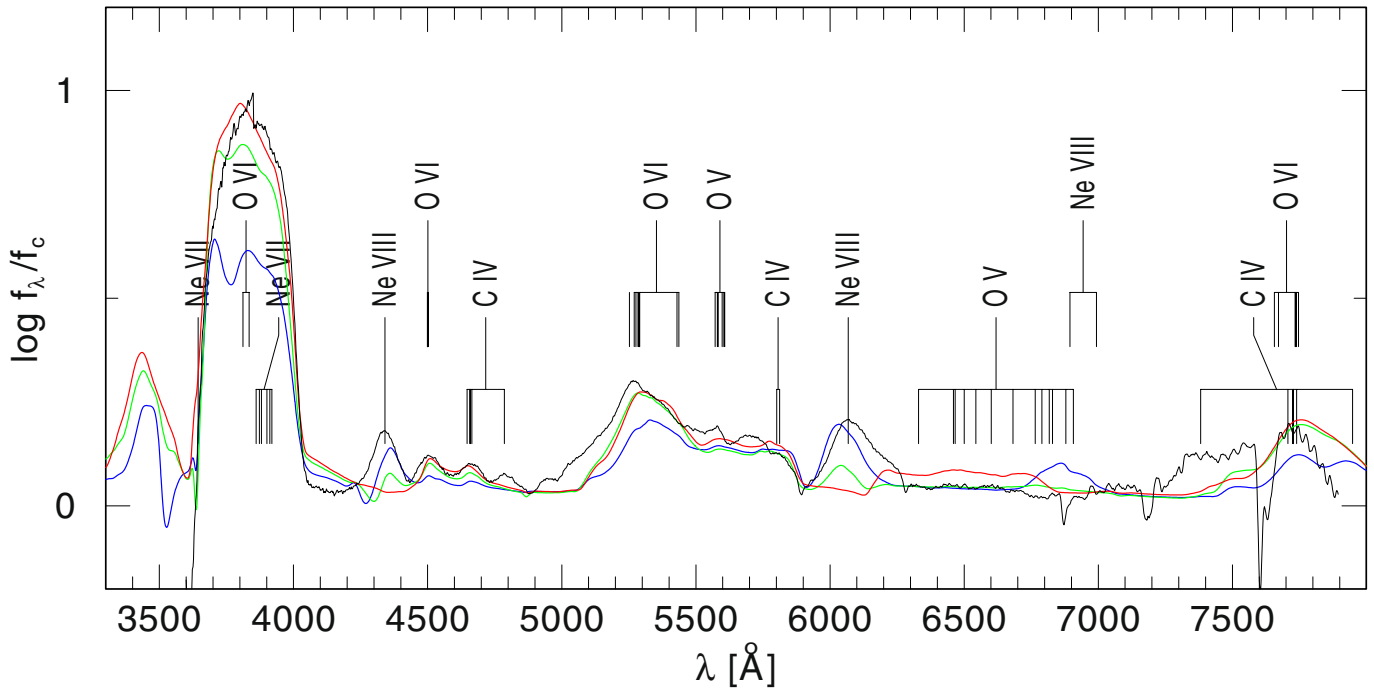

Extended Data Fig. 1 | Neon features in our models. Comparison of models with neon surface mass fractions of 0.0 (red), 0.1 (green) and 0.5 (blue) with observations (black). The observed and calculated fluxes are divided by the same modelled continuum flux f_c.

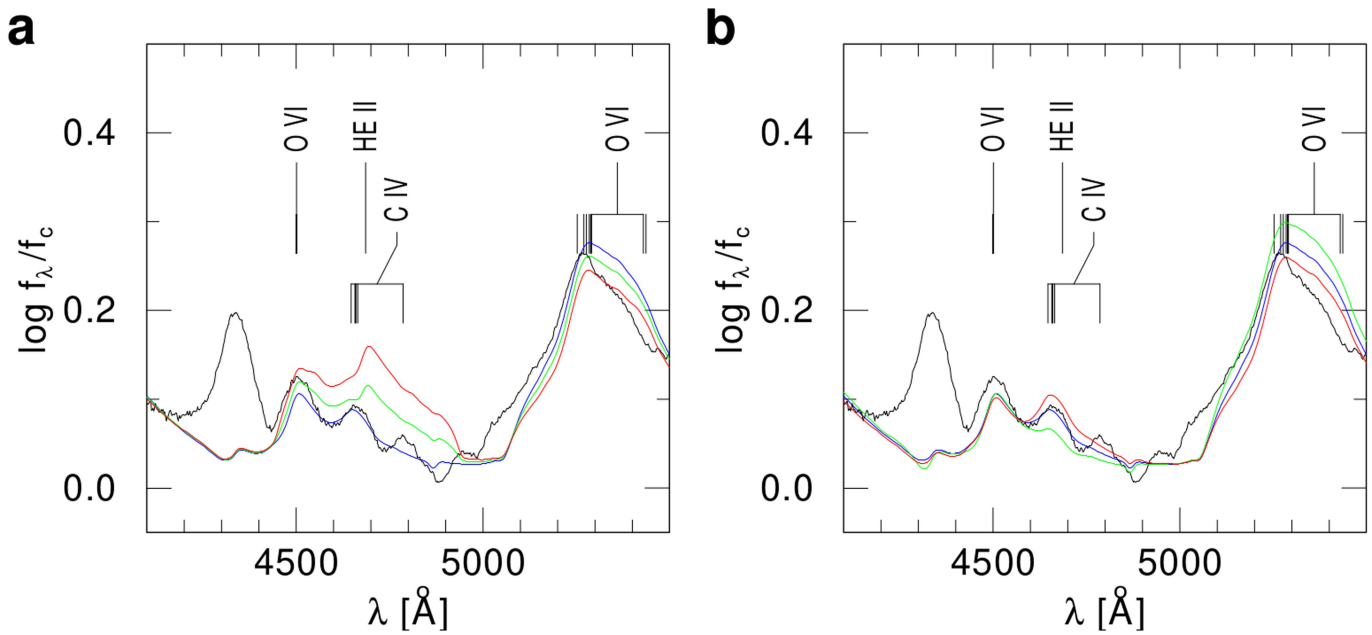

Extended Data Fig. 2 | Abundances. a, Comparison of the observed spectrum of J005311 (black line) with our best-fitting model (helium mass fraction $Y = 0.0$; blue) with models with increased helium abundance ($Y = 0.1$, green; $Y = 0.2$, red). **b**, Comparison of our best-fitting model (carbon mass fraction $X(\mathrm{C}) = 0.2$; blue) with models with altered carbon abundance ($X(\mathrm{C}) = 0.1$, green; $X(\mathrm{C}) = 0.3$, red).

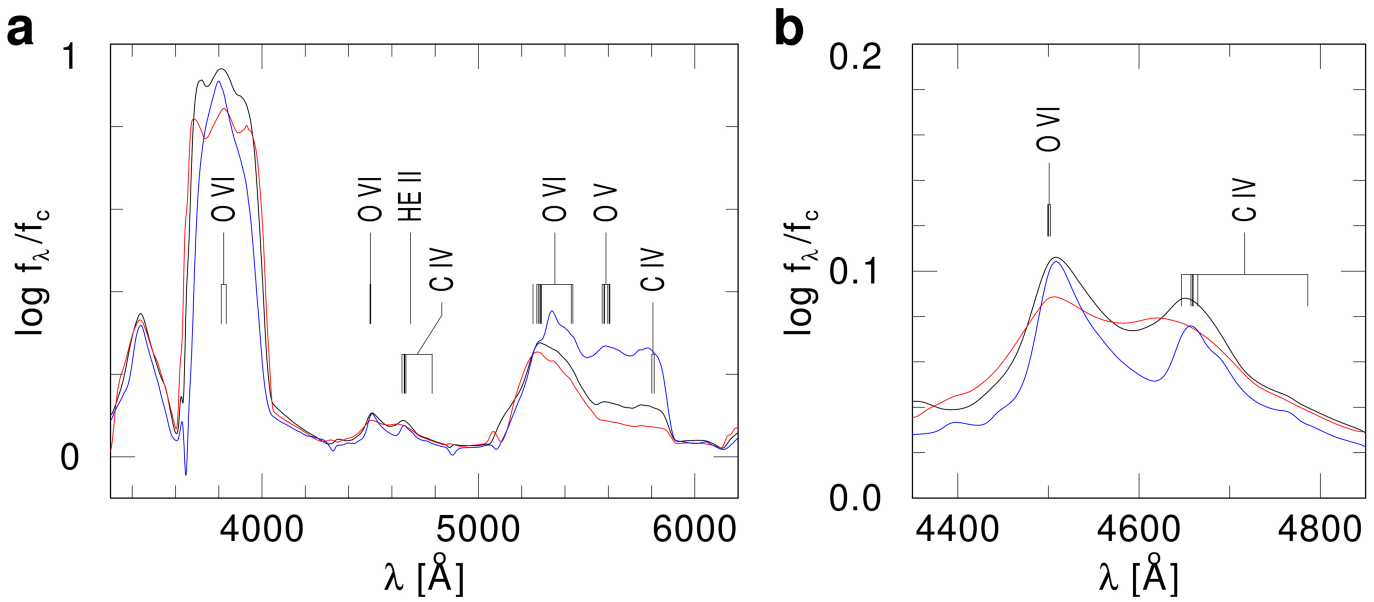

Extended Data Fig. 3 | Stellar temperature. a, Comparison of our best-fitting model (211,000 K; black) with models that are hotter (266,000 K; red) and cooler (178,000 K; blue) than the temperature range given in Table 1. **b**, Magnified profiles of the O VI 4,500 Å and C IV 4,660 Å lines.